


Article

The Au₁₂ Gold Cluster: Preference for a Non-Planar Structure

Pham Vu Nhat ^{1,*}, Nguyen Thanh Si ¹, Nguyen Ngoc Khanh Anh ¹, Long Van Duong ^{2,3} 
and Minh Tho Nguyen ^{4,5,*} ¹ Department of Chemistry, Can Tho University, Can Tho 900000, Vietnam² Laboratory for Computational Molecular and Materials Sciences, Science and Technology Advanced Institute, Van Lang University, Ho Chi Minh City 700000, Vietnam³ Faculty of Applied Technology, School of Engineering and Technology, Van Lang University, Ho Chi Minh City 700000, Vietnam⁴ Department of Chemistry, KU Leuven, B-3001 Leuven, Belgium⁵ Institute for Computational Science and Technology (ICST), Quang Trung Software City, Ho Chi Minh City 700000, Vietnam

* Correspondence: nhat@ctu.edu.vn (P.V.N.); tho.nm@icst.org.vn (M.T.N.)

Abstract: The transition point from a two-dimensional (2D) to a three-dimensional (3D) structure in a series of small gold clusters remains a topic of continuing debate. In the present study, coupled-cluster CCSD(T) and DFT calculations are performed to re-examine the relative energies of several low-lying isomers of Au₁₂, aiming to shed new light on this issue. At odds with many previous reports on the preference of a planar di-capped elongated-hexagon structure, the Au₁₂ size is found to energetically prefer a globular cup-like form with C_{2v} symmetry. While DFT results are not able to assign the most stable form of Au₁₂ as the relative energies between the lowest-lying isomers are strongly functional-dependent, coupled-cluster theory calculations point out the preference of a 3D structure for having a D_{3h} symmetry. Such a prediction is further supported by a comparison of the vibrational spectra computed using the revTPSS density functional with the available experimental infrared ones that were previously recorded from the far-IR multiple photon dissociation (FIR-MPD) experiment.



Citation: Nhat, P.V.; Si, N.T.; Anh, N.N.K.; Duong, L.V.; Nguyen, M.T. The Au₁₂ Gold Cluster: Preference for a Non-Planar Structure. *Symmetry* **2022**, *14*, 1665. <https://doi.org/10.3390/sym14081665>

Academic Editor: Anthony Harriman

Received: 18 July 2022

Accepted: 9 August 2022

Published: 11 August 2022

Publisher's Note: MDPI stays neutral with regard to jurisdictional claims in published maps and institutional affiliations.



Copyright: © 2022 by the authors. Licensee MDPI, Basel, Switzerland. This article is an open access article distributed under the terms and conditions of the Creative Commons Attribution (CC BY) license (<https://creativecommons.org/licenses/by/4.0/>).

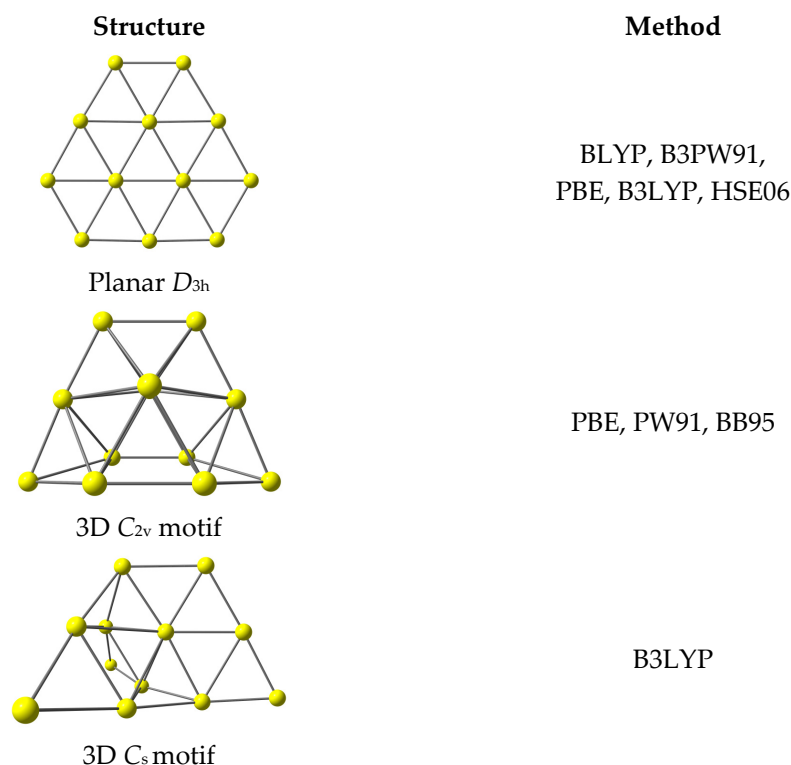
Keywords: gold clusters; Au₁₂; structural transition of gold clusters; FIR spectra; revTPSS functional; coupled-cluster CCSD(T)

1. Introduction

There has been continuing interest in noble metal clusters and nanoparticles owing to their actual and promising applications in, among other things, electronic devices, biochemical sensing and detection, biomedical sciences and nanocatalysis [1–7]. Elucidation of the atomic arrangements and structural evolution of such clusters is a fundamental step in the understanding of their chemical, optical, magnetic and catalytic properties, and also a necessary interplay with other feasible applications. Numerous studies using both theoretical and experimental approaches have been devoted to small gold clusters in recent years with the aim of deciphering their ground-state structures, including the possible lowest-lying isomeric forms of each size and their growth mechanism [8–25].

As a result of a strong relativistic effect, gold clusters exhibit a preference for planar or quasi-planar shapes up to surprisingly large sizes, and a structural transition from planarity to non-planarity mostly occurs in a size between Au₁₀ and Au₁₄ [26]. In a recent theoretical study [27], we demonstrated that a plausible two-dimensional (2D)–three-dimensional (3D) transition of the pure neutral gold clusters likely occurs at the size of Au₁₀, in which both planar and 3D isomers are energetically quasi-degenerate. Concerning the size of Au₁₂, previous investigations proposed several distinct structures as the lowest-lying equilibrium structure of Au₁₂ [16–25]. Scheme 1 displays three 2D and 3D structural motifs that have most frequently been assigned along with the computational methods employed. Most, if not all, of the previous computations were based on density functional theory (DFT),

making use of a variety of functionals that invariably led to conflicting results. In fact, earlier studies reported that some 3D conformations are energetically more stable than their 2D counterparts (cf. Scheme 1) [16,17,20,23]. Other DFT studies pointed out that the Au₁₂ size holds a high symmetry planar D_{3h} equilibrium structure that actually reproduces the Au(111) surface of the metal bulk with slight distortions [18,19,21,28]. More recent computational studies [22,24,25] seemed to lend further support for the preference of a 2D structure (Scheme 1).



Scheme 1. Some structural motifs previously assigned as the most stable isomer of Au₁₂. Results were obtained by density function theory computations using different functionals.

As for other transition metals, gold clusters constitute a rather challenging target for theoretical probes, in part due to the presence of many isomers that nearly degenerate in energy and their inherent characteristics such as relativistic effects. Overall, DFT calculations using different functionals lead to a divergence in the energy ordering of the lowest-lying isomers of Au₁₂ [28]. The lack of reliable spectroscopic information also results in another source for the uncertainty of structural assignments. In fact, assignments of the available experimental spectra were also not always straightforward. Recently, Goldsmith et al. [24] carried out a thorough analysis on the structure of Au₁₂ by comparing the experimental vibrational spectrum recorded from a far-IR multiple photon dissociation (FIR-MPD) spectrometric experiment of the Au₁₂-Kr_n complexes with the theoretical ones simulated from calculated vibrational frequencies for its lowest-lying isomers. These authors [24] found that the theoretical spectrum of the most stable planar form according to the DFT energies they obtained (cf. Scheme 1) does not match the experiment well [24]. Instead, the IR spectrum of a higher-energy isomer, having a 3D shape, provides a better fit, but their conclusion was only tentative on the basis of DFT results.

In view of such a controversy, the present study was carried out, aiming to elucidate the geometrical and spectroscopic features of the neutral Au₁₂ cluster making use of various DFT approaches. As for more convincing evidence on energetic parameters, wave-function-based coupled-cluster theory CCSD(T) [29,30] computations were then performed at the DFT optimized equilibrium geometries. In particular, the IR spectra of Au₁₂ lower-lying isomers are also generated and compared with the experimental data previously recorded

from the far-IR multiple photon dissociation (FIR-MPD) spectrometric experiment [24]. Although several studies have been devoted to the Au clusters functionalized with organic ligands [31], we only consider in the present work the bare gold clusters that are generated in the gas phase and spectroscopically characterized.

2. Computational Methods

Our theoretical data are collected by means of DFT calculations using different density functionals, including the PBE [32], TPSS [33], revTPSS [34] and LC-BLYP [35]. The correlation-consistent aug-cc-pVDZ-PP basis set is employed [36], hereafter denoted as aVDZ-PP, in which PP stands for an effective potential. This is a small-core relativistic pseudopotential [36] in which 60 electrons of the inner shells of the Au atom are treated as a core, and it was developed on the basis of the relativistic potential of Figgen et al. [37]. It is a two-component relativistic PP including the scalar-relativistic and spin-orbit (SO) potentials. As for further evaluation, coupled-cluster theory CCSD(T) [29,30] calculations are also performed at the revTPSS/aVDZ-PP optimized geometries using both cc-pVDZ-PP (VDZ-PP) and cc-pVTZ-PP (VTZ-PP) basis sets. In coupled-cluster theory computations, all 60 core electrons of each Au atom are frozen. The IR spectra of the lowest-lying Au₁₂ isomers are simulated using DFT frequencies and intensities and then compared to the experimental spectra reported in ref. [24]. All electronic structure calculations in this study are performed using the Gaussian 16 [38] and Molpro 2020 [39–41] programs.

3. Results and Discussion

3.1. Equilibrium Structures

Optimized geometries along with symmetry point groups and relative energies (kcal/mol) of the four lowest-lying Au₁₂ isomers are presented in Figure 1, while their Cartesian coordinates are given in Table S1 of the electronic Supplementary Information (SI) file. Figure 1 includes the 2D isomer **Iso_2**, which was commonly assumed as the global energy minimum in the current literature [16–25], and two 3D isomers **Iso_1** and **Iso_3** that were assigned to have the lowest energy in some other studies (cf. Scheme 1).

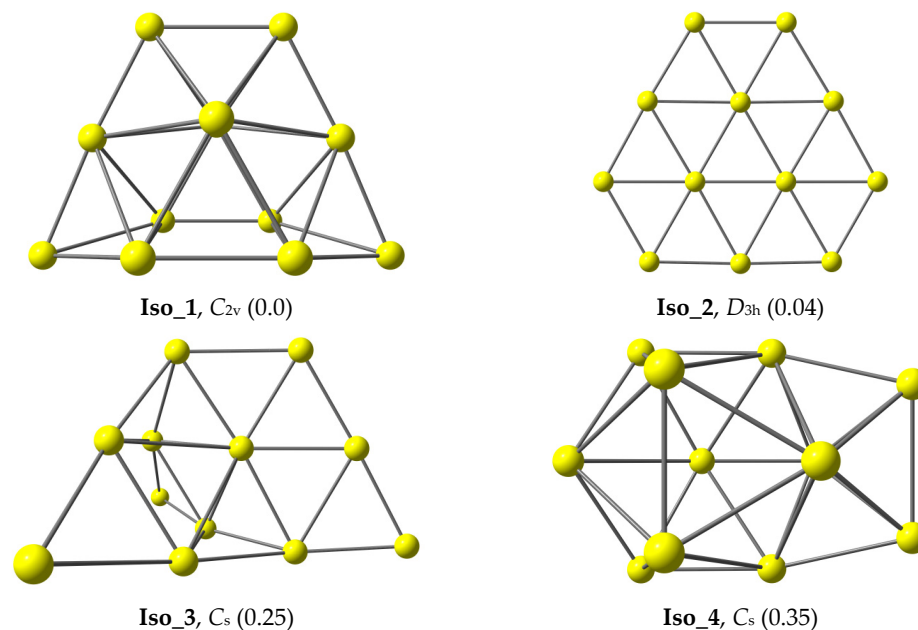


Figure 1. Some low-lying isomers located for the Au₁₂ cluster along with symmetry point group and relative energy with respect to the lowest-lying isomer **Iso_1**. Relative energies given in parentheses are in eV and obtained from CCSD(T)/cc-pVTZ-PP calculations at revTPSS/aug-cc-pVDZ-PP optimized geometries with ZPE corrections.

Our present calculations indicate that the 3D cup-like structure **Iso_1** turns out to be the most stable form of Au₁₂. At the CCSD(T)/cc-pVTZ-PP + ZPE level, the planar di-capped elongated hexagon **Iso_2** is found to be nearly degenerate in energy with **Iso_1**, being only ~1.0 kcal/mol above it. The use of improved basis sets such as the core correlation cc-pwCVTZ-PP or the quadruple-zeta cc-pVQZ-PP tends to confirm the higher stability of the nonplanar **Iso_1**, which remains the lowest-lying isomer of Au₁₂, being lower than the planar **Iso_2** by ~0.09 eV (Table S2 of the Supplementary Materials). In view of the small energy separation between both isomers, lying within the expected error margins of the best computational results, namely ± 0.04 – 0.09 eV of the chemical accuracy, it can be suggested that both isomers are competitive to act as the Au₁₂ ground state. This result thus disagrees with many previous predictions that the 2D **Iso_2** form is the sole equilibrium geometry of Au₁₂ [21,24,25]. The next isomer **Iso_3** that was reported earlier as the global minimum in ref. [20] now has a relative energy of ~0.26 eV higher than **Iso_1**. The remaining 3D isomer, i.e., **Iso_4** in Figure 1, is less stable, being located at ~0.35 eV above the ground state.

Let us mention that the 3D **Iso_1** is also located as the ground state geometry of Au₁₂ by DFT computations using the revTPSS functional. However, as seen in Table 1, calculations using other functionals usually lead to a different energy landscape. The energies of low-lying Au_n isomers are again found to be greatly sensitive in the method employed [23,42,43]. Previous studies have revealed that most DFT approaches tend to overestimate the thermodynamic stability of the planar structure. Our computations using the TPSS and PBE functionals also predict the 2D structure **Iso_2** to possess the lowest energy, whereas the LC-BLYP locates **Iso_4** as the global minimum. Of the four density functionals considered in this study, only the revTPSS yields the same relative energy ordering with respect to the CCSD(T) results that the 3D **Iso_1** is the most stable isomer of Au₁₂. Nonetheless, the revTPSS energy gap between both 3D **Iso_1** and 2D **Iso_2** isomers turns out to be larger with a relative energy of ~0.17 eV.

Table 1. Relative energies (eV) of four lowest-lying Au₁₂ isomers computed at different levels.

Isomer	TPSS	PBE	LC-BLYP	revTPSS	CCSD(T)	
	aVDZ-PP				VDZ-PP	VTZ-PP
Iso_1	0.10	0.36	0.13	0.00	0.00	0.00
Iso_2	0.00	0.00	0.22	0.17	0.52	0.04
Iso_3	0.38	0.74	0.78	0.18	0.11	0.25
Iso_4	0.37	0.41	0.00	0.52	0.41	0.33

In order to include the dispersion corrections, we carry out further calculations using the DFT-D3 functional. Computed results summarized in Table S3 (Supplementary Materials) reveal that the 3D **Iso_1** is consistently more stable than the 2D **Iso_2**. More remarkably, the energy gap between both isomers turns out to be larger at the expense of the 2D isomer. At the revTPSS-D3/aVDZ-PP level, the latter lies ~1 eV above the former (Table S3). Calculated Gibbs energies confirm the nearly degenerate stability of both isomers **Iso_1** and **Iso_2** at temperatures T = 100, 200 and 300 K (cf. free energy ΔG values in Table S4 of the Supplementary Materials). However, this result needs to be regarded with caution. The low values of harmonic frequencies could indeed bias the entropic term. Nonetheless, in view of such low frequencies, anharmonic corrections are also quite small, and could not change the entropy evaluation much.

In the density of states (DOS) of bulk gold, it has been found that while deep levels below -1.0 eV are mostly formed by *d*-orbitals, those near the Fermi level and upper are determined by *s*-orbitals [44]. On the contrary, the partial DOS plots of **Iso_1** and **Iso_2** (Figure S1, Supplementary Materials) reveal the significant contributions of both *d* and *s* orbitals in such regions. More importantly, we in addition find that the planar structure has a much stronger *sd*-hybridization than the globular counterpart (Figure S1). The result is

thus consistent with earlier findings on a correlation between a propensity to favor planar structures of small gold clusters with a strong *sd*-hybridization [16].

We now examine the vibrational signatures of the lower-lying Au₁₂ isomers in comparison to the experimental spectra recently reported by Goldsmith et al. [24]. Accordingly, the cluster was produced via laser ablation and thermalized to ~100 K and then recorded with the presence of messenger Kr atoms. We thus consider the Au₁₂Kr_x (*x* = 1, 2) complexes and find that the Kr atoms tend to anchor on the cornered Au atoms as they are more positively charged than the others (Figure S2). The binding energy of the Kr atom to Au₁₂ amounts to ~0.04 eV (revTPSS/aVDZ-PP). Overall, complexes of **Iso_1** remain more stable than those of **Iso_2**, being ~0.13 eV higher (Figure S3), and the introduction of Kr atoms induces minor changes on the intensities in the low-energy region, while the peak positions remain almost unchanged (Figure S4). Therefore, our analysis on the FIR-MPD spectra is based on the simulated ones of Au₁₂ isomers, as displayed in Figure 2.

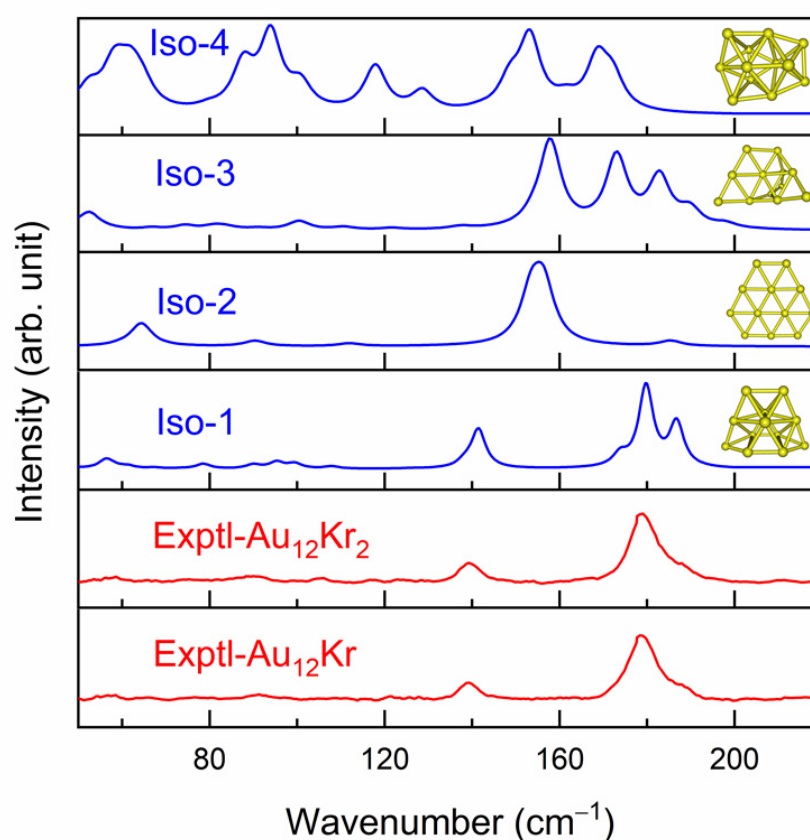


Figure 2. Experimental and theoretical IR spectra of Au₁₂ isomers. Calculated spectra are plotted with a half-width at half-height of 5 cm⁻¹. The experimental FIR spectra are taken from ref. [24]. Simulations are made using harmonic vibrational frequencies (without scaling) and intensities obtained by revTPSS/aug-cc-pVDZ-PP computations.

These results allow a conclusion to be drawn that the 2D isomer **Iso_2** was not the carrier of the experimental vibrational signals. In this context, the 3D **Iso_1** can effectively be assigned as the main carrier of the observed spectrum because it provides us with the best experimental agreement. Accordingly, the highest peak centered at ~180 cm⁻¹ in the computed spectrum of **Iso_1** corresponds to the most intense signal observed experimentally near 180 cm⁻¹. Moreover, this isomer shows a shoulder peak at ~187 cm⁻¹ and a lower intensity signal at ~140 cm⁻¹ that are also all detected experimentally. In contrast, the simulated IR spectra of other 3D isomers, namely **Iso_3** and **Iso_4**, do not match the experiment at all (Figure 2).

In ref. [24], the 3D **Iso_1** was also suggested to be mostly responsible for the observed spectrum of Au₁₂, albeit it is not the lowest-energy form obtained from DFT computations using the PBE and HSE06 functionals. It can be argued that calculations using the current DFT functionals have led to another energy ordering of the 2D/3D crossover in the Au₁₂ system. Most of these density functionals can emphasize the very small energy differences between the lowest-lying isomers at a certain size of gold cluster, but they are not able to accurately reveal the identity of the most stable form.

Recent FIR-MPD measurements combined with DFT calculations have confirmed that the open-shell Au₁₁ system tends to exhibit a non-planar conformation, i.e., **11_2** in Figure 3, in its ground state [24]. In the present study, we find two lowest-lying isomers competing for the equilibrium geometry of Au₁₁ that are displayed in Figure 3. At the revTPSS/aVDZ-PP + ZPE level, **11_1** is found to be 0.1 eV more stable than **11_2**. The same energy ordering is also found by (U)CCSD(T)/aVDZ-PP + ZPE calculations but with a larger energy gap of 0.2 eV in favor of the former. The most stable form **Iso_1** of Au₁₂ is indeed obtained by adding one extra Au atom to the lowest-lying isomer **11_1** of the smaller-sized Au₁₁. Such an evolution, which forms the basis for the successive growth algorithm for the structural search, lends further support for the preference of the 3D structure **Iso_1** over its 2D counterpart **Iso_2**.

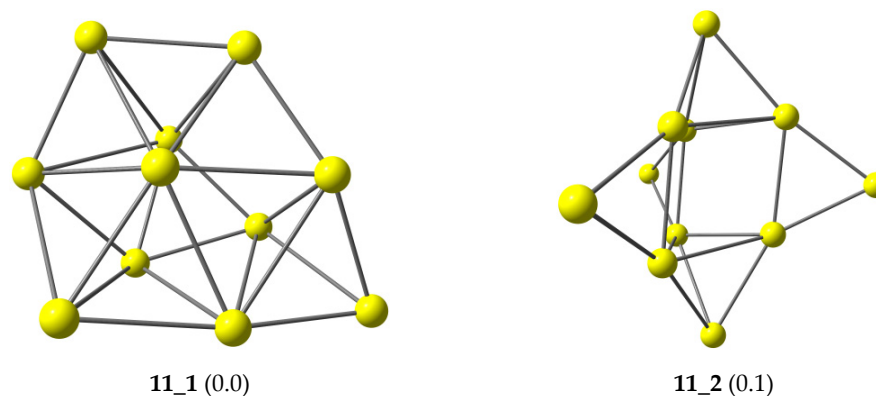


Figure 3. Two lowest-lying isomers competing for the ground-state structure of the Au₁₁ cluster. Values given in parentheses are their relative energy in eV (revTPSS/aVDZ-PP + ZPE).

To further evaluate the dynamic stability of the isomer, we carry out some ab initio molecular dynamic (AIMD) simulations [43] for both 3D **Iso_1** and 2D **Iso_2** isomers with a time scale of 2.0 ps at 100, 200 and 298 K, in view of the fact that the clusters are experimentally generated in low-temperature beams. Figure S5 (Supplementary Materials) shows the potential energy variations subject to the simulation times. At temperatures below 298K, the potential energies of both 3D and 2D isomers are not significantly varied, suggesting that they have a high thermodynamic stability with this temperature range.

3.2. Electronic Properties

Plots of the frontier orbitals, including HOMO and LUMO, of **Iso_1** and **Iso_2** isomers are presented in Figure 4. At the revTPSS/aug-cc-pVDZ-PP level, such states of both structures are nearly degenerated in energy. The energies of the HOMO and LUMO in **Iso_1** amount to -0.162 and -0.197 a.u., respectively, which are comparable with the corresponding values of -0.164 and -0.202 a.u. in **Iso_2**. As a result, the total electronic energies of these forms turn out to be almost the same.

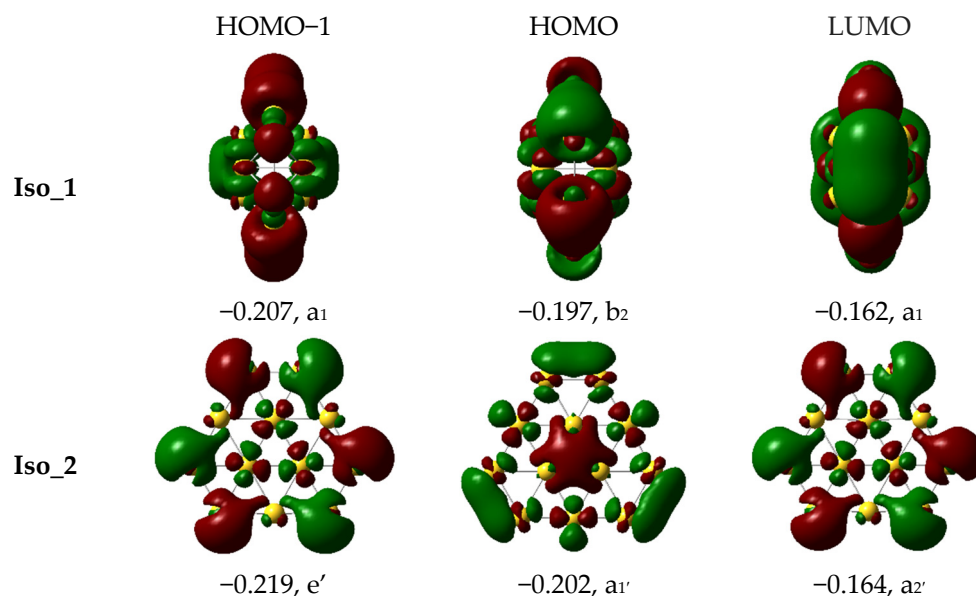


Figure 4. Energy (a.u.) and symmetry of frontier orbitals in **Iso_1** and **Iso_2** isomers and their energies (values in parentheses in a.u.; revTPSS/aVDZ-PP).

As for a supplement of energetic data, the vertical ionization energies (IE_v), vertical electron affinities (EA_v) and first vertical excitation energies for the $S_0 \rightarrow S_1$ transition of the four isomers considered are listed in Table 2. The IE_v of the neutral Au_{12} is calculated by taking the geometry of the vertical cation to be the same as the optimized neutral, whereas the EA_v refers to the value obtained at its optimized neutral structure for the vertical anion. Using the revTPSS functional combined with the aug-cc-pVTZ-PP basis set, we find that the ability to donate and accept an electron of both planar and nonplanar isomers are comparable. The IE_v values of **Iso_1** and **Iso_2** are predicted to be 7.0 and 7.1 eV, respectively, while the corresponding EA_v values amount to 2.8–2.9 eV (Table 2), which are rather large electron affinities. Similarly, a tiny difference is also observed for the first vertical excitation energies in the UV–visible absorption spectra of **Iso_1** and **Iso_2** (cf. Table 2). These results are rather particular as both IE and EA values of clusters tend to be altered with respect to not only the size, but also the shape [44].

Table 2. Vertical ionization energies (IE_v), vertical electron affinities (EA_v) and the first vertical excitation energy ($S_0 \rightarrow S_1$ transition) of Au_{12} 's lowest-lying isomers (revTPSS/aVDZ-PP).

	IE_v , eV	EA_v , eV	Energy of $S_0 \rightarrow S_1$ Transition, eV
Iso_1	7.01	2.80	1.06
Iso_2	7.07	2.90	1.08
Iso_3	7.09	2.78	1.24
Iso_4	6.94	2.79	0.95

The optical properties of gold clusters attract a great deal of interest owing to their importance in both basic and applied research, and thus have been the subject of numerous studies using both experimental and computational approaches alike [45–48]. However, as far as we are aware, the experimental UV spectrum for Au_{12} is not available yet. Calculations performed for both 2D and 3D isomers using the time-dependent density-functional theory (TD-DFT) with the revTPSS functional and aug-cc-pVTZ-PP basis set show that the absorption spectrum of the 3D **Iso_1** contains some particularly strong transitions between 435 and 465 nm (Figure 5), along with lower intensity peaks near 500 nm. The 2D **Iso_2** exhibits a more symmetric spectrum with a sharper band at ~440 nm. Figure 4 also reveals that the planar isomer **Iso_2** absorbs the light in the visible region much better than its

3D counterparts. Let us mention that TD-DFT calculations using the revTPSS functional tend to underestimate the $S_0 \rightarrow S_1$ transition energy as compared to those including the long-range exchange effects. For the planar **Iso_2**, such a transition observed at 1.1 eV by the revTPSS is smaller than the corresponding value of 1.3 eV located previously with the LC- ω PBEh functional [48].

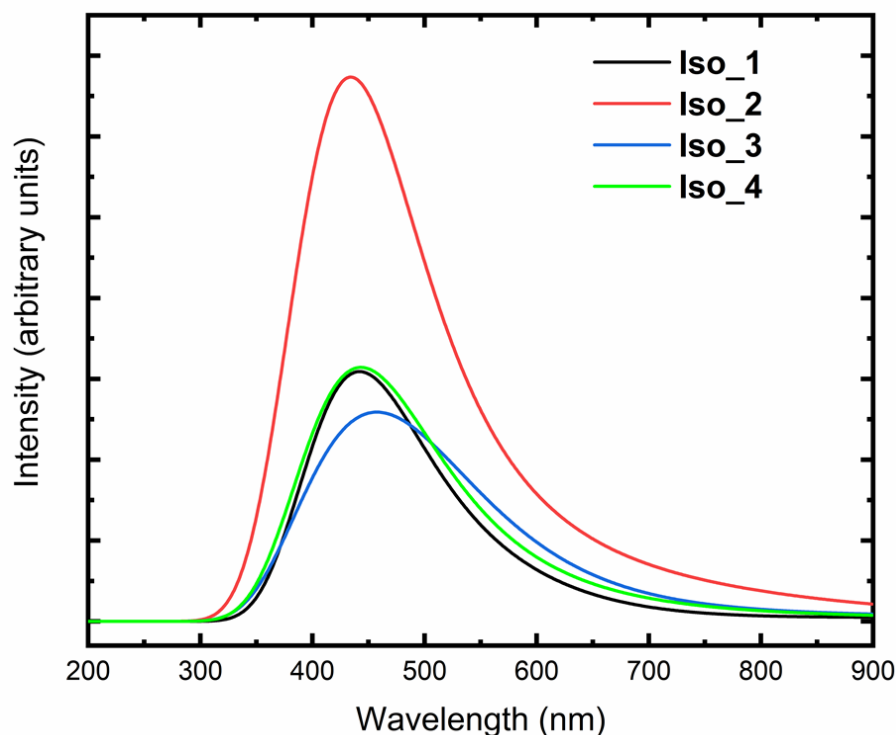


Figure 5. Computed absorption spectra (TD-DFT/revTPSS/aVTZ-PP) for the lowest-lying isomers of Au_{12} . The spectra are plotted with a half-width at half-height of 0.2 eV.

4. Concluding Remarks

In summary, high-accuracy coupled-cluster CCSD(T) calculations revealed that, at odds with many previous reports, the neutral gold cluster Au_{12} tends to exhibit a 3D conformation in its ground state. The global energy minimum of such a small gold cluster cannot reliably be assigned by relying merely on DFT energetic results as the relative energies between the lowest-lying isomers are greatly dependent on the functional employed. Of the four density functionals employed, the revTPSS is found to reach closer to the CCSD(T) results for relative energies than either the TPSS, PBE or LC-BLYP. Experimental information, namely vibrational spectra, plays a crucial role in providing us with more persuasive evidence on the identity of the cluster geometry in its ground state. Indeed, a comparison of simulated IR spectra of lower-lying Au_{12} isomers with those obtained from the FIR-MPD experiment ($Au_{12}Kr_n$ complexes) clearly support a preference of the 3D cup-like isomer over the others. Along with our recent results [27] that revealed a likely coexistence of both 2D and 3D structures of Au_{10} , a preference for a 3D isomer at the size of Au_{12} reinforces the view that the onset of the planar–nonplanar structural transition of pure gold clusters Au_n likely occurs at the size of $n \sim 10$.

Supplementary Materials: The following supporting information can be downloaded at: <https://www.mdpi.com/article/10.3390/sym14081665/s1>.

Author Contributions: Conceptualization, P.V.N.; Data curation, N.T.S. and N.N.K.A.; Formal analysis, N.T.S. and L.V.D.; Funding acquisition, M.T.N.; Investigation, N.T.S. and N.N.K.A.; Methodology, P.V.N. and L.V.D.; Supervision, M.T.N.; Validation, M.T.N.; Writing—original draft, P.V.N.; Writing—review and editing, M.T.N. All authors have read and agreed to the published version of the manuscript.

Funding: This work is funded by VinGroup (Vietnam) and supported by VinGroup Innovation Foundation (VinIF) under project code VinIF.2020.DA21.

Institutional Review Board Statement: Not applicable.

Informed Consent Statement: Not applicable.

Data Availability Statement: Data are given in the Supplementary Materials.

Acknowledgments: We greatly appreciate valuable discussion with André Fielicke at the Fritz-Haber Institute Berlin, Germany, on the assignment of their experimental infrared spectra of gold clusters reported in ref. [24]. LVD is thankful to the Van Lang University.

Conflicts of Interest: The authors declare no conflict of interest.

References

- Schmid, G. Nanoclusters—building blocks for future nanoelectronic devices? *Adv. Eng. Mater.* **2001**, *3*, 737–743. [[CrossRef](#)]
- Loth, S.; Baumann, S.; Lutz, C.P.; Eigler, D.M.; Heinrich, A.J. Bistability in atomic-scale antiferromagnets. *Science* **2012**, *335*, 196–199. [[CrossRef](#)] [[PubMed](#)]
- Saha, K.; Agasti, S.S.; Kim, C.; Li, X.; Rotello, V.M. Gold nanoparticles in chemical and biological sensing. *Chem. Rev.* **2012**, *112*, 2739–2779. [[CrossRef](#)] [[PubMed](#)]
- Austin, L.A.; Mackey, M.A.; Dreaden, E.C.; El-Sayed, M.A. The optical, photothermal, and facile surface chemical properties of gold and silver nanoparticles in biodiagnostics, therapy, and drug delivery. *Arch. Toxicol.* **2014**, *88*, 1391–1417. [[CrossRef](#)]
- Teles, J.H.; Brode, S.; Chabanas, M. Cationic gold (I) complexes: Highly efficient catalysts for the addition of alcohols to alkynes. *Angew. Chem. Int. Ed. Engl.* **1998**, *37*, 1415–1418. [[CrossRef](#)]
- Veenboer, R.M.; Dupuy, S.; Nolan, S.P. Stereoselective gold (I)-catalyzed intermolecular hydroalkoxylation of alkynes. *ACS Catal.* **2015**, *5*, 1330–1334. [[CrossRef](#)] [[PubMed](#)]
- Rudolph, M.; Hashmi, A.S.K. Heterocycles from gold catalysis. *Chem. Commun.* **2011**, *47*, 6536–6544. [[CrossRef](#)]
- Collings, B.A.; Athanassenas, K.; Rayner, D.M.; Hackett, P.A. Optical spectroscopy of Ag_7 , Ag_9^+ , and Ag_9 . A test of the photodepletion method. *Chem. Phys. Lett.* **1994**, *227*, 490–495. [[CrossRef](#)]
- Krückeberg, S.; Dietrich, G.; Lützenkirchen, K.; Schweikhard, L.; Walther, C.; Ziegler, J. The dissociation channels of silver clusters Ag_n^+ , $3 \leq n \leq 20$. *Int. J. Mass Spectrom.* **1996**, *155*, 141–148. [[CrossRef](#)]
- Shayeghi, A.; Götz, D.A.; Johnston, R.L.; Schäfer, R. Optical absorption spectra and structures of Ag_6^+ and Ag_8^+ . *Eur. Phys. J. D* **2015**, *69*, 152. [[CrossRef](#)]
- Yang, X.; Cai, W.; Shao, X. Structural variation of silver clusters from Ag_{13} to Ag_{160} . *J. Phys. Chem. A* **2007**, *111*, 5048. [[CrossRef](#)] [[PubMed](#)]
- Fournier, R. Theoretical study of the structure of silver clusters. *J. Chem. Phys.* **2001**, *115*, 2165–2177. [[CrossRef](#)]
- Bonačić-Koutecky, V.; Veyret, V.; Mitrić, R. Ab initio study of the absorption spectra of ($n = 5–8$) clusters. *J. Chem. Phys.* **2001**, *115*, 10450–10460. [[CrossRef](#)]
- Chen, M.; Dyer, J.E.; Li, K.; Dixon, D.A. Prediction of structures and atomization energies of small silver clusters, $(\text{Ag})_n$, $n < 100$. *J. Phys. Chem. A* **2013**, *117*, 8298–8313. [[PubMed](#)]
- Jin, Y.; Tian, Y.; Kuang, X.; Zhang, C.; Lu, C. Ab initio search for global minimum structures of pure and boron doped silver clusters. *J. Phys. Chem. A* **2015**, *119*, 6738–6745. [[CrossRef](#)]
- Fernández, E.M.; Soler, J.M.; Garzón, I.L.; Balbás, L.C. Trends in the structure and bonding of noble metal clusters. *Phys. Rev. B* **2004**, *70*, 165403. [[CrossRef](#)]
- Li, X.-B.; Wang, H.-Y.; Yang, X.-D.; Zhu, Z.-H.; Tang, Y.-J. Size dependence of the structures and energetic and electronic properties of gold clusters. *J. Chem. Phys.* **2007**, *126*, 084505. [[CrossRef](#)]
- Deka, A.; Deka, R.C. Structural and electronic properties of stable Au_n ($n = 2–13$) clusters: A density functional study. *J. Mol. Struct.* **2008**, *870*, 83–93. [[CrossRef](#)]
- Assadollahzadeh, B.; Schwerdtfeger, P. A systematic search for minimum structures of small gold clusters Au_n ($n = 2–20$) and their electronic properties. *J. Chem. Phys.* **2009**, *131*, 064306. [[CrossRef](#)]
- Zanti, G.; Peeters, D. DFT Study of Bimetallic Palladium–Gold Clusters Pd_nAu_m of Low Nuclearities ($n + m \leq 14$). *J. Phys. Chem. A* **2010**, *114*, 10345–10356. [[CrossRef](#)]
- Mukhamedzyanova, D.F.; Ratmanova, N.K.; Pichugina, D.A.; Kuz'menko, N.E. A Structural and Stability Evaluation of Au_{12} from an Isolated Cluster to the Deposited Material. *J. Phys. Chem. C* **2012**, *116*, 11507–11518. [[CrossRef](#)]
- Kinaci, A.; Narayanan, B.; Sen, F.G.; Davis, M.J.; Gray, S.K.; Sankaranarayanan, S.K.R.S.; Chan, M.K.Y. Unraveling the Planar-Globular Transition in Gold Nanoclusters through Evolutionary Search. *Sci. Rep.* **2016**, *6*, 34974. [[CrossRef](#)] [[PubMed](#)]
- Nhat, P.V.; Si, N.T.; Leszczynski, J.; Tho, N.M. Another look at structure of gold clusters Au_n from perspective of phenomenological shell model. *Chem. Phys.* **2017**, *493*, 140–148. [[CrossRef](#)]

24. Goldsmith, B.R.; Florian, J.; Liu, J.-X.; Gruene, P.; Lyon, J.T.; Rayner, D.M.; Fielicke, A.; Scheffler, M.; Ghiringhelli, L.M. Two-to-three dimensional transition in neutral gold clusters: The crucial role of van der Waals interactions and temperature. *Phys. Rev. Mater.* **2019**, *3*, 016002. [[CrossRef](#)]
25. Persaud, R.R.; Chen, M.; Dixon, D.A. Prediction of Structures and Atomization Energies of Coinage Metals, $(M)_n$, $n < 20$: Extrapolation of Normalized Clustering Energies to Predict the Cohesive Energy. *J. Phys. Chem.* **2020**, *124*, 1775–1786. [[CrossRef](#)]
26. Johansson, M.P.; Warnke, I.; Le, A.; Furche, F. At What Size Do Neutral Gold Clusters Turn Three-Dimensional? *J. Phys. Chem. C* **2014**, *118*, 29370–29377. [[CrossRef](#)]
27. Nhat, P.V.; Si, N.T.; Hang, N.T.N.; Nguyen, M.T. The lowest-energy structure of the gold cluster Au₁₀: Planar vs. nonplanar? *Phys. Chem. Chem. Phys.* **2022**, *24*, 42–47. [[CrossRef](#)]
28. Baker-Austin, C.; McArthur, J.V.; Tuckfield, R.C.; Najarro, M.; Lindell, A.H.; Gooch, J.; Stepanauskas, R. Antibiotic resistance in the shellfish pathogen *Vibrio parahaemolyticus* isolated from the coastal water and sediment of Georgia and South Carolina, USA. *J. Food Prot.* **2008**, *71*, 2552–2558. [[CrossRef](#)]
29. Rittby, M.; Bartlett, R.J. An open-shell spin-restricted coupled cluster method: Application to ionization potentials in nitrogen. *J. Phys. Chem.* **1988**, *92*, 3033–3036. [[CrossRef](#)]
30. Knowles, P.J.; Hampel, C.; Werner, H.J. Coupled cluster theory for high spin, open shell reference wave functions. *J. Chem. Phys.* **1993**, *99*, 5219–5227. [[CrossRef](#)]
31. Hossain, S.; Nair, L.V.; Inoue, J.; Koyama, Y.; Kurashige, W.; Negishi, Y. *Ligand-Protected Gold Clusters, in Ligand*; IntechOpen: London, UK, 2018.
32. Perdew, J.P.; Burke, K.; Ernzerhof, M. Generalized gradient approximation made simple. *Phys. Rev. Lett.* **1996**, *77*, 3865. [[CrossRef](#)] [[PubMed](#)]
33. Tao, J.; Perdew, J.P.; Staroverov, V.N.; Scuseria, G.E. Climbing the density functional ladder: Nonempirical meta-generalized gradient approximation designed for molecules and solids. *Phys. Rev. Lett.* **2003**, *91*, 146401. [[CrossRef](#)] [[PubMed](#)]
34. Perdew, J.P.; Ruzsinszky, A.; Csonka, G.I.; Constantin, L.A.; Sun, J. Workhorse Semilocal Density Functional for Condensed Matter Physics and Quantum Chemistry. *Phys. Rev. Lett.* **2009**, *103*, 026403. [[CrossRef](#)] [[PubMed](#)]
35. Iikura, H.; Tsuneda, T.; Yanai, T.; Hirao, K. A long-range correction scheme for generalized-gradient-approximation exchange functionals. *J. Chem. Phys.* **2001**, *115*, 3540–3544. [[CrossRef](#)]
36. Peterson, K.A.; Puzzarini, C. Systematically convergent basis sets for transition metals. II. Pseudopotential-based correlation consistent basis sets for the group 11 (Cu, Ag, Au) and 12 (Zn, Cd, Hg) elements. *Theor. Chem. Acc.* **2005**, *114*, 283–296. [[CrossRef](#)]
37. Figgen, D.; Rauhut, G.; Dolg, M.; Stoll, H. Energy-consistent pseudopotentials for group 11 and 12 atoms: Adjustment to multi-configuration Dirac–Hartree–Fock data. *Chem. Phys.* **2005**, *311*, 227–244. [[CrossRef](#)]
38. Frisch, M.J.; Trucks, G.W.; Schlegel, H.B.; Scuseria, G.E.; Robb, M.A.; Cheeseman, J.R.; Scalmani, G.; Barone, V.; Petersson, G.A.; Nakatsuji, H.; et al. *Gaussian 16 Rev. B.01*; Gaussian, Inc.: Wallingford, CT, USA, 2016.
39. Werner, H.J.; Knowles, P.J.; Knizia, G.; Manby, F.R.; Schütz, M. Molpro: A general-purpose quantum chemistry program package. *Wiley Interdiscip. Rev. Comput. Mol. Sci.* **2012**, *2*, 242–253. [[CrossRef](#)]
40. Werner, H.J.; Knowles, P.J.; Manby, F.R.; Black, J.A.; Doll, K.; Heßelmann, A.; Kats, D.; Köhn, A.; Korona, T.; Kreplin, D.A. The Molpro quantum chemistry package. *J. Chem. Phys.* **2020**, *152*, 144107. [[CrossRef](#)]
41. Werner, H.J.; Knowles, P.J.; Knizia, G.; Manby, F.R.; Schütz, M.; Celani, P.; Györffy, W.; Kats, D.; Korona, T.; Lindh, R.; et al. The Molpro quantum chemistry package. *J. Chem. Phys.* **2020**, *152*, 144107. [[CrossRef](#)]
42. Zhumagulov, Y.V.; Kashurnikov, V.; Krasavin, A. Calculation of electron density of states for ensemble of gold nanoclusters. *J. Phys. Conf. Ser.* **2017**, *936*, 012015. [[CrossRef](#)]
43. Du, J.; Sun, X.; Jiang, G. Hydrogen storage capability of cagelike Li₃B₁₂ clusters. *J. Appl. Phys.* **2020**, *127*, 054301. [[CrossRef](#)]
44. Tho, N.H.; Bui, T.Q.; Si, N.T.; Nhat, P.V.; Nhung, N.T.A. Structural characteristics and chemical reactivity of gold-based clusters Au_n ($n = 16, 17$) toward lone pairs. *J. Mol. Model.* **2022**, *28*, 54. [[CrossRef](#)] [[PubMed](#)]
45. Idrobo, J.C.; Walkosz, W.; Yip, S.F.; Ögüt, S.; Wang, J.; Jellinek, J. Static polarizabilities and optical absorption spectra of gold clusters (Au n , $n = 2–14$ and 20) from first principles. *J. Phys. Rev. B* **2007**, *76*, 205422. [[CrossRef](#)]
46. Liao, M.-S.; Bonifassi, P.; Leszczynski, J.; Ray, P.C.; Huang, M.-J.; Watts, J.D. Structure, bonding, and linear optical properties of a series of silver and gold nanorod clusters: DFT/TDDFT studies. *J. Phys. Chem. A* **2010**, *114*, 12701–12708. [[CrossRef](#)]
47. Lecoultrre, S.; Rydlo, A.; Félix, C.; Buttet, J.; Gilb, S.; Harbich, W. UV–visible absorption of small gold clusters in neon: Au n ($n = 1–5$ and $7–9$). *J. Chem. Phys.* **2011**, *134*, 074302. [[CrossRef](#)]
48. Koppen, J.V.; Hapka, M.; Szcześniak, M.M.; Chałasiński, G. Optical absorption spectra of gold clusters Au_n ($n = 4, 6, 8, 12, 20$) from long-range corrected functionals with optimal tuning. *J. Chem. Phys.* **2012**, *137*, 114302. [[CrossRef](#)]